Water Research X 5 (2019) 100037

Contents lists available at ScienceDirect

Water Research X

journal homepage: https://www.journals.elsevier.com/water-research-x

Model-based assessment of chromate reduction and nitrate effect in a methane-based membrane biofilm reactor

Zhen Wang [a], Xue-Ming Chen [b], Bing-Jie Ni [c], You-Neng Tang [d], He-Ping Zhao [a, *]

[a] MOE Key Lab of Environmental Remediation and Ecosystem Health, College of Environmental and Resource Science, Zhejiang University, Hangzhou, 310058, China
[b] Process and Systems Engineering Center (PROSYS), Department of Chemical and Biochemical Engineering, Technical University of Denmark, Kgs Lyngby, 2800, Denmark
[c] College of Environmental Science and Engineering, Tongji University, Shanghai, China
[d] FAMU-FSU College of Engineering, Florida State University, Tallahassee, USA

ARTICLE INFO

Article history:
Received 12 March 2019
Received in revised form
9 September 2019
Accepted 21 September 2019
Available online 15 October 2019

Keywords:
Membrane biofilm reactor
Chromate reduction
Nitrate effect
Aerobic methane oxidation
Model analysis

ABSTRACT

Chromate contamination can pose a high risk to both the environment and public health. Previous studies have shown that CH_4-based membrane biofilm reactor (MBfR) is a promising method for chromate removal. In this study, we developed a multispecies biofilm model to study chromate reduction and its interaction with nitrate reduction in a CH_4-based MBfR. The model-simulated results were consistent with the experimental data reported in the literature. The model showed that the presence of nitrate in the influent promoted the growth of heterotrophs, while suppressing methanotrophs and chromate reducers. Moreover, it indicated that a biofilm thickness of 150 μm and an influent dissolved oxygen concentration of 0.5 mg O_2/L could improve the reactor performance by increasing the chromate removal efficiency under the simulated conditions.

1. Introduction

Chromium is an important raw metal material and is used in various industries such as metallurgy. Moreover, it can be used as refractories or for leather tanning. Discharge of inadequately treated wastewater from these industrial sites leads to the presence of excess chromium in water and soil. Chromium mainly occurs in the Cr(VI) and Cr(III) states. Uptake of Cr(VI) can alter the germination and root growth processes of plants and jeopardize their physiological processes (Shanker et al., 2005). Furthermore, inhalation of Cr(VI) leads to nasal septum perforation, asthma, pneumonitis, and bronchogenic carcinoma in mammals. The maximum contaminant level (MCL) for Cr was set at 100 μg/L for drinking water by the US EPA (2009). On the other hand, Cr(III) is an essential element for humans (Srivastava et al., 1999). The recommended intake for chromium is 20–35 μg/day for adults (Floch, 2013). Furthermore, Cr(III) is less soluble and more easily removed from liquid phases. Thus, the reduction of Cr(VI) to Cr(III) represents a promising method to solve the chromium contamination problem.

Previous studies have shown that Cr(VI) can be reduced to Cr(III) by different microorganisms (Camargo et al., 2003; Pattanapipitpaisal et al., 2001; Zhai et al., 2017). Recently, Lai et al. (2016a) reported successful Cr(VI) reduction in a membrane biofilm reactor (MBfR), in which methane diffused through the non-porous membrane serving as the sole electron donor for the biofilm. Meanwhile, Cr(VI) diffused from the bulk liquid into the biofilm, where microbial-mediated chromate reduction took place. The counter diffusion biofilm supported a unique microbial ecology (Nerenberg, 2016). Considering the fact that the greenhouse gas methane is cost-effective and widely available, a CH_4-based MBfR is a promising option for the removal of Cr(VI) (Lai et al., 2016b; Long et al., 2017; Luo et al., 2015; Lv et al., 2019; Modin et al., 2008).

The performance of the MBfR can be affected by operational conditions such as inoculum, gas pressure, biofilm thickness management strategies, and the loading of co-existing electron acceptors such as dissolved oxygen and nitrate (Nerenberg et al., 2002; Tang et al., 2010). It is unclear how these conditions interact and affect the removal of chromate. Moreover, answering this question requires tremendous experimental efforts. In contrast, multispecies biofilm modeling can be a powerful and

* Corresponding author.
E-mail address: zhaohp@zju.edu.cn (H.-P. Zhao).

https://doi.org/10.1016/j.wroa.2019.100037

convenient tool for quantitative analysis and reactor optimization (Lackner et al., 2008; Tang et al., 2013). Therefore, the first objective of this study was to develop a multispecies biofilm model to analyze the chromate removal efficiency of the CH_4-based MBfR. Due to the countercurrent diffusion at the biofilm in the MBfR, the biofilm thickness profoundly influences the performance of the MBfR. Therefore, the second objective of this study was to understand the effect of dissolved oxygen (DO), which significantly affects the thickness of the biofilm, on MBfR performance. Zhong et al. (2017) found that nitrate and chromate interacted with each other in the MBfR, with nitrate greatly reducing the rate of chromate reduction. Nitrate is a common contaminant in wastewater, which may affect chromate reduction through the following interactions: i) the competition between nitrate and chromate for the same resources, e.g., methane; ii) the competition for space in the biofilm between different kinds of microorganisms; iii) the promotion of growth of chromate-reducing microorganisms through their utilization of nitrate (Tang et al., 2012). The extent to which nitrate influences chromate reduction depends on the loading rates of both nitrate and chromate. Therefore, the third objective of this study was to explore the performance of the CH_4-based MBfR under various combinations of chromate and nitrate loading rates.

2. Model development and evaluation

2.1. Model development

Cr(VI) and nitrate reduction coupled to methane oxidation has been reported to occur mainly via an indirect pathway, in which methane is firstly oxidized by methanotrophs into intermediates which are then utilized by other microorganisms to reduce electron acceptors such as chromate, nitrate, and oxygen. In the model developed by Modin et al. (2018), aerobic methanotrophs utilized methane and expelled methanol, which was used by heterotrophs to reduce oxygen and nitrate. Long et al. (2017) identified methanotrophs, denitrifiers, and Cr(VI) reducers in a methane- and oxygen-based MBfR. Moreover, our group (Lai et al., 2016a) also found methanotrophs, chromate reducers, and denitrifiers in the CH_4-based MBfR. Therefore, we proposed the following model.

The model contains 5 solid species and 6 soluble species. The solids species are methane oxidizing bacteria (X_{AMO}), heterotrophic bacteria (X_{HB}), chromate reducing bacteria (X_{CRB}), inert biomass (X_{IB}), and extracellular polymeric substances (X_{EPS}). The soluble species are methane (S_{CH4}), methanol (S_{CH3OH}), oxygen (S_{O2}), chromate (S_{CrO4}), nitrate ($S_{\bar{N}O3}$), substrate utilization-associated products (S_{UAP}), and biomass-associated products (S_{BAP}). Specific information is listed in Table S1 in the SI.

The critical biological processes considered in the model are displayed in Fig. 1. In the biofilm, CH_4 is consumed by the AMO by reducing O_2 in the inflow. The oxidation product, methanol, then serves as the electron donor for the reduction of chromate (by CRB) and nitrate (by CRB and HB). UAP and EPS are produced during the growth process of the microorganisms. EPS is then hydrolyzed to biomass-associated products (BAP), while UAP and BAP serve as electron donors for HB. All microorganisms are subject to endogenous respiration, in which they are oxidized by corresponding electron acceptors and partially converted to inert biomass (Laspidou and Rittmann, 2002). Methane diffuses into the biofilm from the hollow fiber membrane wall, while other soluble species diffuse into the biofilm from the bulk liquid. In contrast, the solid products become part of the biofilm. The soluble products first diffuse into the pore water in the biofilm, then into the bulk liquid, and finally leave the system together with the effluent.

2.2. Model assumptions and simplifications

For further biofilm modeling, several simplification and assumptions were made.

1) The MBfR biofilm model was based on the one-dimension biofilm model developed by Wanner and Reichert (1996). The biofilm was modeled as a continuum with the components changing only in the direction perpendicular to the membrane surface. The biomass was described as quantity per volume (Wanner and Gujer, 1986). The one-dimension biofilm assumption was widely used to predict the overall reactor performance (Chen and Ni, 2016; Chen et al., 2016; Sun et al., 2017).
2) The kinetics of the biological reactions was described using dual-substrate Monod kinetics. The inhibition observed in the experiment was modeled as a noncompetitive form according to Activated Sludge Model (Henze et al., 2000; Tekerlekopoulou et al., 2013; Peng et al., 2016). Moreover, the substrate diffusion was simulated according to Fick's law. The specific rate of expression and the stoichiometry are listed in Tables S2 and S3.1–3.5 in the SI.
3) The methane flux from the fiber lumen to the biofilm base was depicted as a diffusive process driven by the concentration gradient. The flux was described as follows:

$$I_{CH4} = q_{ex,CH4}\left(\frac{S_{CH4,1}}{H_{CH4}} - S_{CH4,2}\right)$$

Where $S_{CH4,1}$ and $S_{CH4,2}$ are gas concentrations of methane in the fiber lumen and biofilm-membrane interface (kg-COD/m^3); $q_{ex,CH4}$ is the overall mass exchange coefficient of methane (m^2/day); and H_{CH4} is Henry's coefficient for methane (kg-COD m^{-3} gas/kg-COD m^{-3} liquid). The methane pressure in the lumen is converted to COD concentration by using the ideal gas equation.

4) The thickness of the diffusion layer was 100 μm, with the biofilm having a porosity of 0.6 and a density of 100000 g-COD/m^3 (Horn and Lackner, 2014).
5) The contribution of the suspended solids was ignored in the system. Moreover, the pH of the system was maintained at 7.0–7.5; thus, the effect of pH was not considered (Sun et al., 2017).

The detachment occurred on the biofilm-bulk liquid interface. The composition of the detached biomass was consistent with that of the biofilm interface. No attachment or reattachment occurred in the reactor (Ni and Yuan, 2013; Ni et al., 2013; Tang et al., 2012).

6) The steady state was obtained by controlling the global detachment velocity, which is a second-order function of the biofilm thickness (Ni et al., 2013).

The CH_4-based MBfR was modeled using two compartments of the AQUASIM 2.1g, a software designed for the modeling of aquatic systems (Reichert, 1994). The biofilm and bulk liquid were modeled as a biofilm system, while the hollow fiber lumen was modeled as a mixed reactor system. For laboratory configurations, the membrane fiber length was generally less than 35 cm. Moreover, the reactor was in completely mixed condition as it had limited volume and recirculation was used. As such, the mixed reactor assumption was adequate for modeling (Ahmed and Semmens, 1992; Martin and Nerenberg, 2012). The methane flux through hollow fiber membrane wall was modeled by diffusion between the two systems (Reichert, 1998).

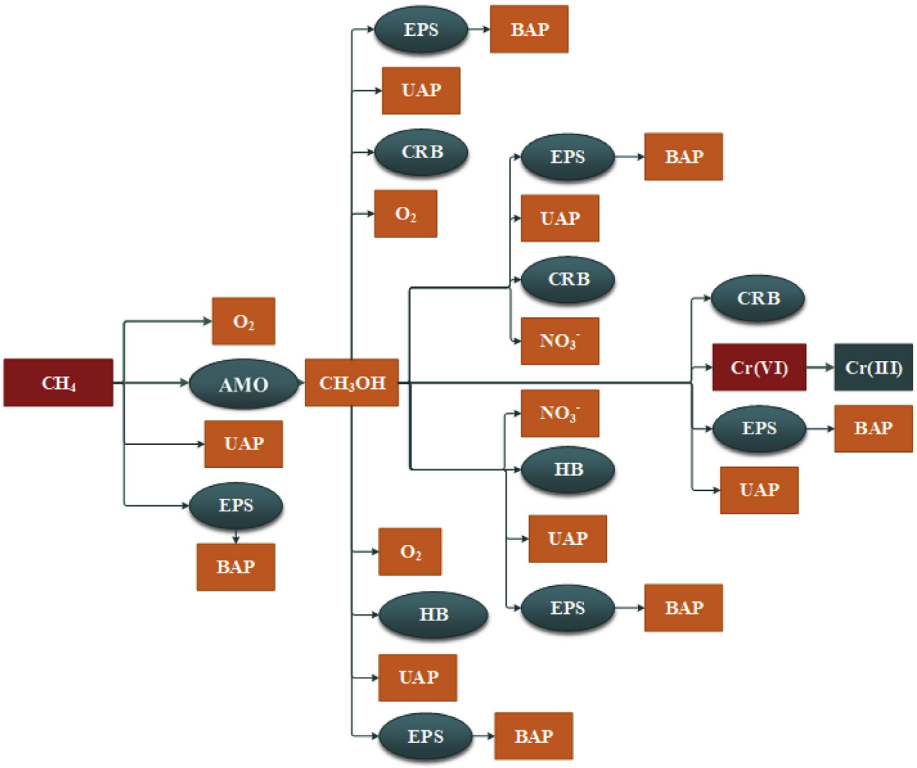

Fig. 1. The electron flow in microbial processes considered in this model.

2.3. Model calibration and validation

The developed biofilm model consists of 17 microbial processes and 35 kinetic/stochiometric parameters. The values of the major parameters are adapted from previous studies (see SI). Specific parameter values and references are listed in Table S4.1 in SI. The kinetic and stoichiometry parameters (maximum growth rates and yield coefficients) were calculated using methods previously described by Rittmann and Mccarty (2002) and summarized in Table S4.2. Three unavailable parameters ($K_{XCRB,CrO4}$, $\mu_{XHB,S}$, η_{CrO4}) were estimated by fitting the experimental data. Sensitivity analysis results are shown in Figs. S1 and S2. According to the results, the AMO-related parameters (Y, μ) and CRB (μ, K_{CrO4}, Y_{CrO4}) related parameters are the most sensitive. Both the parameter estimation and model validation were carried out using the AQUASIM 2.1g software.

2.4. Experimental data used for evaluating the developed model

The experimental data used for model validation was adapted from Lai et al. (2016a) and Zhong et al. (2017). Briefly, the MBfR consisted of a 65 mL tube and a 58 cm^2 composite hollow fiber membrane. The MBfR was operated at a flow rate of 0.5 mL/min (HRT=130 min) and various CH_4 pressures. Five operation conditions were used to explore the chromate removal capacity of the reactor. In a similar experiment, six other stages were carried out to investigate the effect of nitrate on chromate reduction in a CH_4-based MBfR. For each stage, the MBfR reached a steady state according to the effluent concentrations of CrO_4^{2-} and NO_3^-. We selected 5 steady-effluent stages to calibrate the model. Specific effluent concentration values are listed in Table S5. More details can be found in Lai et al. (2016a) and Zhong et al. (2017). We used stages 1, 2, 3, and 5 to calibrate the model and stages 4 and 6 to validate the model.

2.5. Model-based analysis of the microbial community in the biofilm

The performance of the MBfR changed significantly following the introduction of nitrate in the system. We chose 3 experimental stages (4, 5, and 6) to study the microbial distribution in the biofilm. Moreover, the distribution of each species along the vertical direction was simulated, using the AQUASIM 2.0g software. Then, the model output was used to analyze how nitrate affected the distribution of solid species in the biofilm.

2.6. The impact of key operational parameters on chromate removal efficiency

The validated model was then used to investigate the effect of biofilm thickness and influent DO concentration on chromate/nitrate removal in the CH_4-based MBfR. Furthermore, the effect of loading rates of CrO_4^{2-} and NO_3^- were also investigated with the model. The simulated MBfR had a reactor volume of 5 L and a membrane surface area of 0.5 m^2. The reactor area to volume ratio (A/V) was typical for MBfR systems (Sun et al., 2017).

To evaluate the effect of biofilm thickness, the MBfR was simulated with a biofilm thickness ranging from 50 to 800 μm. To evaluate the effect of influent DO concentration, the MBfR was simulated with DO ranging from 0 to 2.0 mg-O_2/L. To evaluate the effect of nitrate on chromate reduction, the MBfR was simulated with various combinations of chromate and nitrate loading rates. The specific simulation scenarios are shown in Table S6 (scenario 1–3).

3. Results and discussion

3.1. Results of model calibration and validation

The experimental data summarized in Table S5 were used to carry out parameter estimation and model validation. The effluent concentrations and removal fluxes from the experiments and the model were compared in Fig. 2 (A-D).

Fig. 2A & B show the influent and effluent concentrations of chromate and nitrate from the experiments and the model. The model results and the experimental results were found to be generally consistent. In stages 1–4, the chromate in the influent was almost completely reduced, resulting in a high removal efficiency (higher than 97% in both the experiments and the model). The Cr(VI) removal flux simulated by the model in stages 1–4 was 116, 228, 370, and 493 mg-Cr/(L·d), respectively. These results are also comparable to the experimental results (117, 231, 367, and 494 mg-Cr/(L·d), respectively). However, the experimental data show that chromate reduction was strongly inhibited in stage 5 (compared to the same chromate loading in stage 4) when 2.2 mg-N/L (24 mg-N/L·d) of nitrate was introduced in the influent. The effluent Cr(VI) concentration increased from approximately 0.8 mg/L to 3.48 mg/L, resulting in a decrease in removal efficiency from 98% to less than 10%. The Cr(VI) reduction percentage was recovered to 62.8% after the nitrate concentration decreased to 0.66 mg/L (7.3 mg/L·d) in stage 6. The model shows very similar results (62.8% of Cr(VI) removal in stage 6 and 11.5% in stage 5). By using previously well-established parameters for methanotrophs, heterotrophs (Sun et al., 2017; Lin et al., 2009), and the proposed metabolic pathways (Chen and Ni, 2016; Tang et al., 2013), the model developed in this study satisfactorily predicted the experimental performance.

3.2. Microbial distribution in the biofilm

The experimental studies have shown that high nitrate loading (24 mg-N/L·d) strongly inhibited chromate removal (Zhong et al., 2017). To understand how nitrate affected chromate removal in the MBfR, we used the validated model to investigate the microbial compositions at stages 4, 5, and 6. Fig. 3A–C show the simulated microbial distribution along the direction perpendicular to the substratum at stage 4 (0 mg-N/L), 5 (24 mg-N/L·d), and 6 (7.3 mg-N/L··d), respectively. Fig. 3 D-F show the overall distribution of biomass in the three stages, respectively. The model-calibrated abundance of microorganisms generally captured the trends of the experimental data, as shown in Figure S3.1-3.3. As shown in Fig. 3A and D, in the absence of nitrate, the biomass was mainly composed of AMO (46%) and CRB (33%). Sun et al. (2017) developed a model for perchlorate reduction in the CH_4-based MBfR and found that methanotrophs were more likely situated close to the membrane. Our model indicated that the AMO were almost uniformly distributed across the biofilm. This was probably caused by the high efficiency of methane transfer of the membrane and the high methane concentrations across the biofilm. When 24 mg-N/L·d of nitrate was added to the influent in stage 5, the steady-state microbial composition changed significantly. The abundance of HB increased from less than 3% to 51.4% in the steady-state, making HB the dominant functional group in the biofilm. Meanwhile, the EPS decreased from 17% to 12%. There might be two explanations for this phenomenon. First, HB had an advantage over CRB due to the

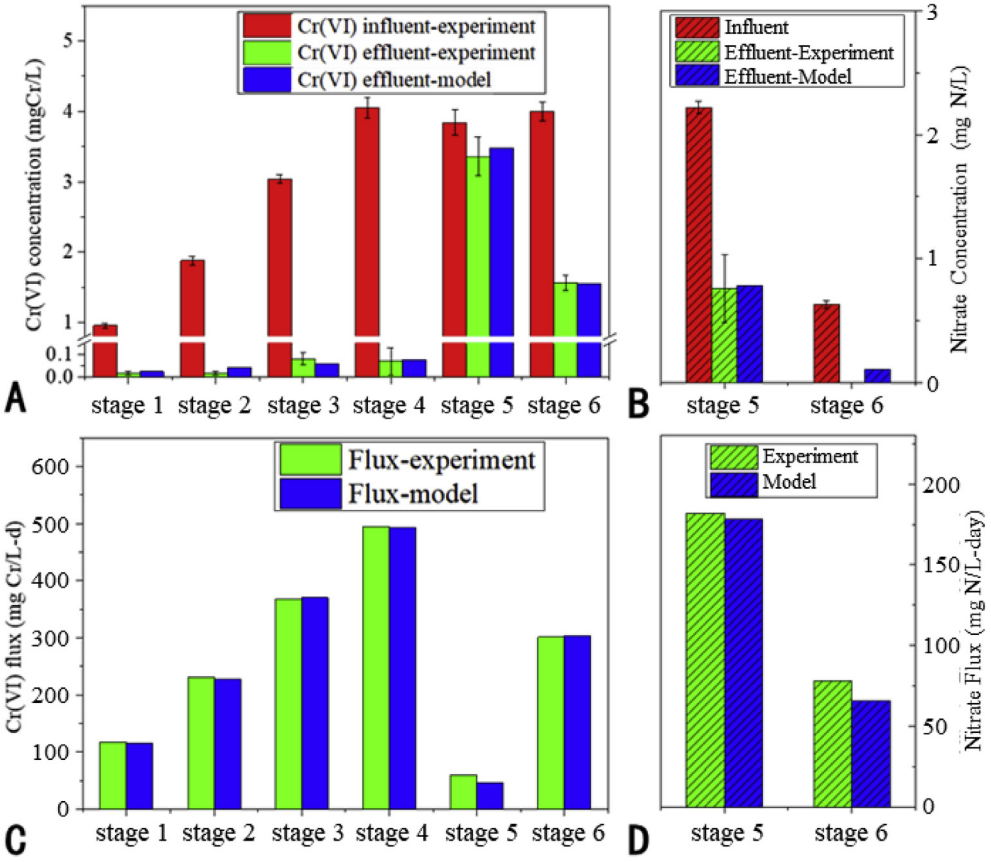

Fig. 2. The concentrations and fluxes of chromate and nitrate from experiments and the model.

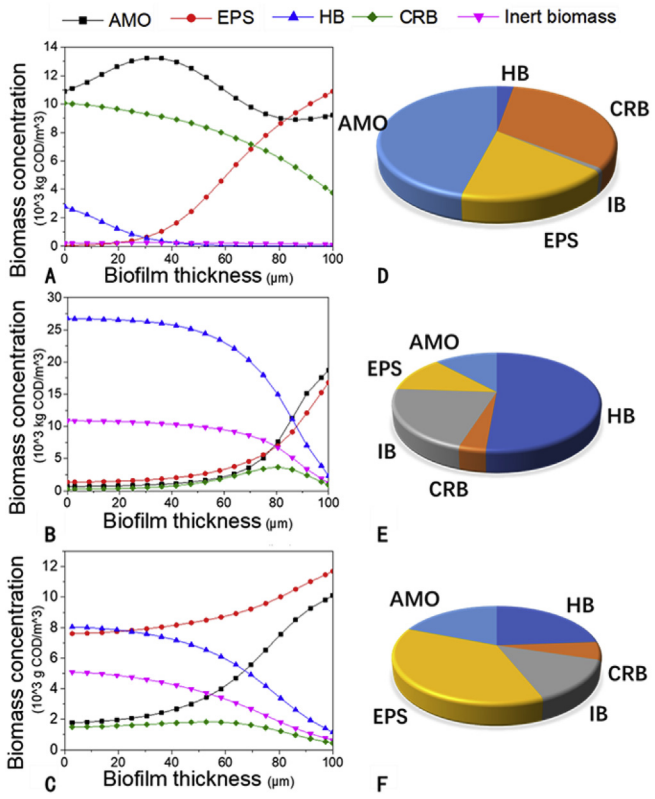

Fig. 3. Biomass concentration distribution and composition of solid species in the steady-state biofilm for stage 4 (A&D, without nitrate), stage 5 (B&E, 24 mg/L·d of nitrate loading), and stage 6 (C&F, 7.3 mg/L·d of nitrate loading).

HB's ability to utilize nitrate. Second, HB could utilize BAP and UAP generated by EPS hydrolysis (Laspidou and Rittmann, 2002). With the increase of HB, CRB was outcompeted for growth space, methanol, and possibly reductase enzymes. As a result, the steady-state fraction of CRB decreased accordingly, the chromate reduction was strongly decreased, and the competition for electrons between chromate and nitrate became fiercer. As shown in Fig. 3C and F, a lower concentration of nitrate of 0.66 mg/L increased the EPS percentage from 12% to 33%. Similarly, Lai et al. (2018) reported that the amount of EPS decreased after a higher loading of vanadate (10 mg/L in influent). Since EPS didn't act as a straight electron donor for chromate reduction, the increase of EPS did not contribute to the reduction of chromate (Liu et al., 2017). It can be inferred that the high concentration of nitrate inhibited chromate reduction, possibly by promoting the competition for electrons between nitrate and chromate, which restricted the electron flow to the chromate. Moreover, low concentrations of nitrate inhibited chromate reduction, possibly via the promotion of EPS secretion. The increase of EPS not only intensified the competition for space but also reduced the rate of chromate diffusion into the biofilm.

3.3. Effect of biofilm thickness and influent DO on chromate removal

Experimental results showed that the MBfR reactor could completely remove up to 44 mg-Cr/L·d of chromate when nitrate was not present. Without testing a higher loading of Cr(VI), the maximum chromate removal capacity of the reactor remained unknown. Since the biofilm thickness could be managed by flow velocity and shear stress, we investigated the reactor performance under various biofilm thicknesses using the developed model. Fig. 4A shows that the fluxes of Cr(VI) and nitrate were more severely affected when the biofilm thickness ranged between 50 and 100 μm, and less affected when the biofilm thickness exceeded 100 μm. This can be explained by substrate diffusion and biomass retention. When the biofilm was thin (less than 100 μm in this case), the reduction was limited by the biomass quantity. Thus, the overall reduction capacity increased with the increase in biofilm thickness. When the biofilm was thicker (more than 150 μm in this case), the reduction was restrained at substrate diffusion. Skowlund (1990) presented a numerical simulation for the biofilm and found that the active biofilm would finally reach a constant value in spite of the increase in biofilm thickness. This might also explain why the efficiency of chromate removal did not continue to increase after the biofilm thickness reached 100 μm.

Methane and oxygen were supplied separately from two sides of the biofilm. The dual substrates limitation more likely occurred when the methane supply was not sufficient, limiting the growth of AMO. In addition, it was less likely that the substrate (Cr(VI)) from the liquid side would be able to penetrate the biofilm, which resulted in waste of the interior biomass. Fig. 4B and C show the simulated biomass distribution for the two biofilm thicknesses (100 μm for B and 500 μm for C). The thicker biofilm promoted the growth of AMO and inert biomass, which outcompeted other microorganisms for space.

Oxygen had dual effects on the reactor efficiency. On the one hand, O_2 is an essential substrate for methane oxidation (generating methanol for chromate and nitrate reduction). On the other hand, oxygen may negatively affect the reactor performance by competing with chromate and nitrate for methanol, the common electron donor. According to Lai et al. (2016b), methane wasn't a limiting factor for methane oxidation in the experiments.

As shown in Fig. 5A, the removal of chromate and nitrate kept increasing along with the increase of influent DO. Fig. 5B and C show the simulated biomass distribution at two DO concentrations (0.5 mg/L for B and 1 mg/L for C). The higher DO promoted the growth of AMO and HB substantially. Similarly, CRB growth was also slightly promoted by the introduction of oxygen. This could be due to higher methanol production due to a higher DO. Although high concentrations of oxygen might compete as an electron acceptor, its adverse effects were not apparent in the simulations. In the experiments, oxygen could only enter the system through the influent (i.e. 0.7 mg-O_2/L), corresponding to a loading rate of 0.504 mg-O_2/d, which could oxidize methane into 0.756 mg COD/d of methanol. This was far away from meeting the needs for chromate and nitrate reduction in the system. Following that, we calculated the potential oxygen intrusion by using reactor-part connectors as described by Alrashed et al. (2018). The results showed that the total DO could reach 3.6 mg-O_2/d, thereby generating 5.1 mg-COD/d, which can meet the demands for the actual chromate and nitrate fluxes in the experiments. The calculation step is detailed in the SI.

3.4. MBfR performance under various combinations of chromate and nitrate loading rates

Nitrate co-exists with chromate in many bodies of water (Chen and Strous, 2013). The experimental results suggested that nitrate affected the reduction of chromate in the CH_4-based MBfR system. Conversely, chromate was also shown to have some impact on nitrate removal (Zhong et al., 2017). Thus, the influence of chromate and nitrate loading on chromate reduction in the CH_4-based MBfR was simulated using the developed model.

Fig. 6A shows the efficiency of chromate removal under various combinations of nitrate and chromate loading rates. The white

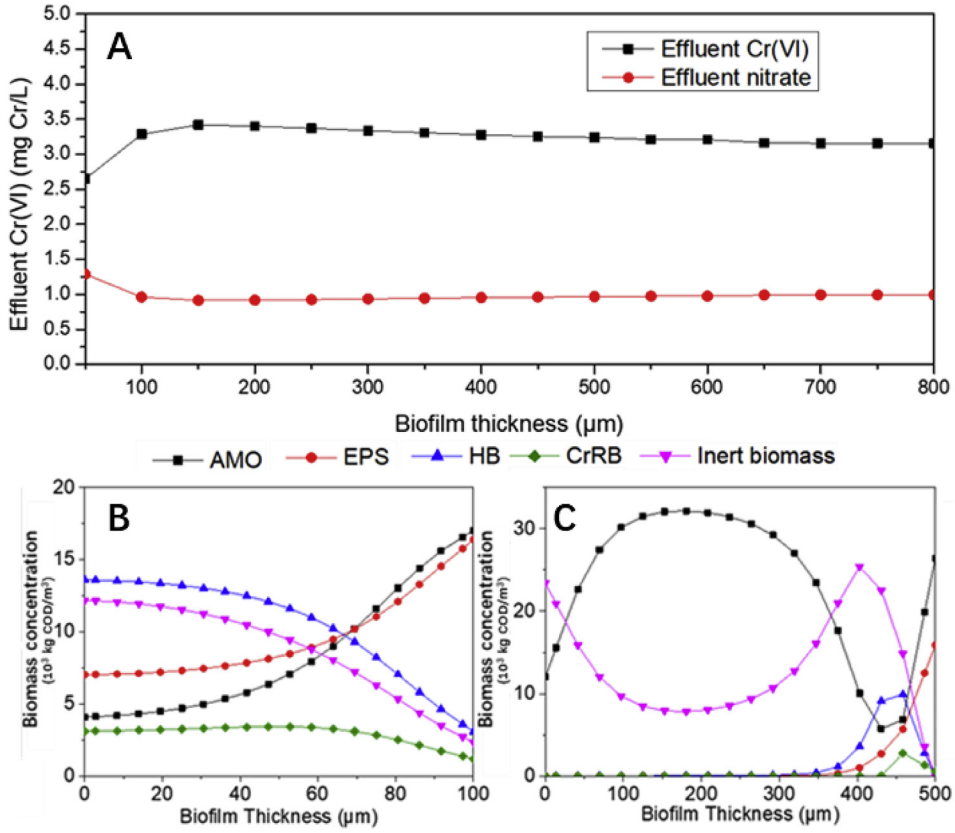

Fig. 4. Effluent nitrate and Cr(VI) concentrations under different biofilm thicknesses (A), and biomass distribution under two sample biofilm thicknesses (B: 100 μm; C: 500 μm).

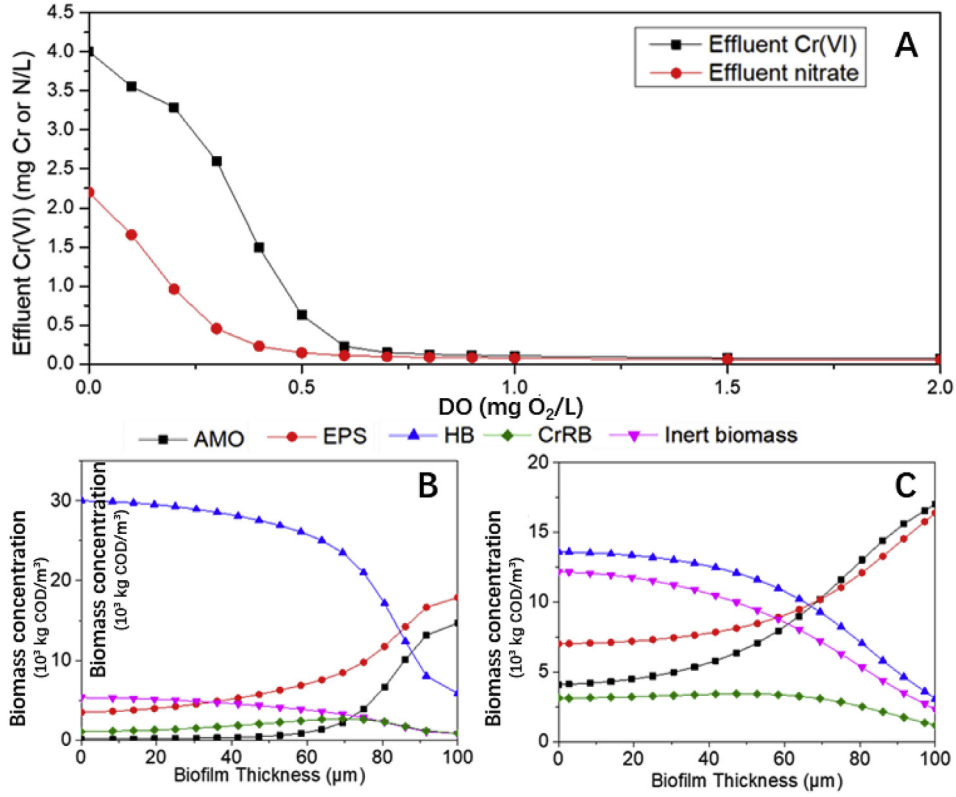

Fig. 5. Effluent nitrate and Cr(VI) concentrations under various influent DO concentrations (A), and biomass distribution under two sample influent DO concentrations (B:0.5 mg-O_2/L; C:1 mg-O_2/L).

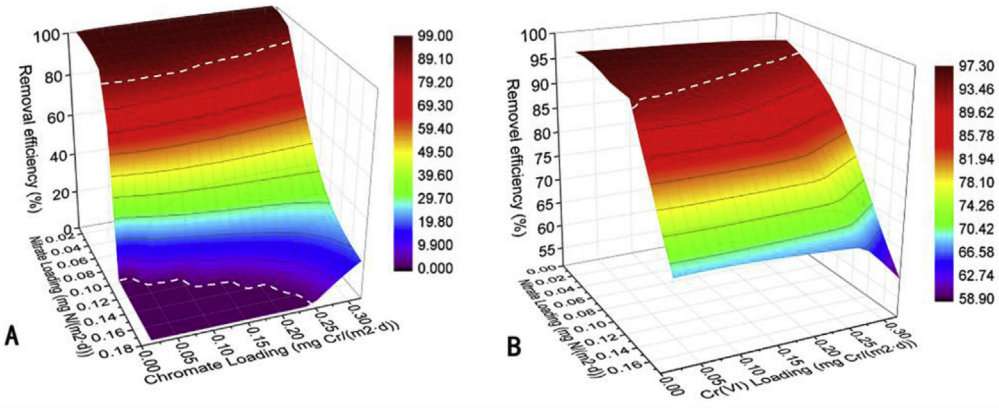

Fig. 6. Reactor performance under various combinations of chromate and nitrate loading rates (A: chromate removal efficiency, B: nitrate removal efficiency).

dotted lines separated the chromate efficiency into three parts. Under low nitrate loading (0–0.04 mg-N/m^2·d), the nitrate had limited inhibition effects on chromate removal efficiency, which remained higher than 80%. Under moderate nitrate loading (0.04–0.10 mg-N/m^2·d), the effect of nitrate become stronger and the chromate removal efficiency declined rapidly with the increase in nitrate levels. This phenomenon was clearly observed even at a low chromate loading. The chromate removal efficiency reached zero in the third part, probably due to the fact that the ability of chromate to compete for electrons was further weakened.

Fig. 6B shows the efficiency of nitrate removal under various combinations of nitrate and chromate loading rates. When chromate was not present in the influent, the nitrate removal efficiency was between 70–97%. Unlike the chromate removal, nitrate removal was more likely affected by its own loading. Under low nitrate loadings (0–0.06 mg N/m^2·d), the nitrate removal efficiency was generally higher than 85%. When the nitrate loading increased to more than 0.06 mg N/m^2-d, the nitrate removal efficiency dropped rapidly from 85% to 67%. However, the introduction of chromate (0–0.30 mg-Cr/m^2·d) led to little inhibition (less than 5% efficiency decrease) of nitrate removal. Generally, the chromate removal flux in the CH_4-based MBfR was very sensitive to nitrate loading, probably because of the advantage of nitrate on the affinity coefficient. As such, the effect of nitrate should be considered in the reactor design. Moreover, a CrO_4^{2-}/NO_3^- ratio may be used as an index for reactor design, similarly to the NO_2^-/NH_4^+ ration for designing the MBfR carrying out denitrification coupled to anaerobic methane oxidation (Chen et al., 2016)

3.5. Practical implication

Excessive chromate in bodies of water can pose potential risks both to the environment and public health. As chromate and nitrate often co-occur in wastewater and the standards for nitrate are usually a few magnitudes higher than those for chromate, knowledge about alleviating the effect of nitrate on chromate removal is of practical importance. Removal of chromate from water, based on the CH_4-based MBfR, has been demonstrated by previous experiments. This study systematically investigated the effect of nitrate on chromate removal. It is expected that the developed model and the simulated results could be a reference for the reactor design. Further evaluation of the model using a wider range of operation conditions is needed. Some mechanical factors such as fluid dynamics and shear stress should also be taken into account when the model is applied in pilot or bigger scale tests.

4. Conclusion

In this study, we developed a biofilm model for chromate and nitrate reduction in the CH_4-based MBfR. The model-simulated results fitted the experimental data satisfactorily. The model was then used to analyze the effect of nitrate on chromate removal in MBfR. The model analysis revealed that nitrate exacerbated the competition among AMOs, HBs, and chromate reducers. Moreover, HBs were promoted while AMO and chromate reducers (CRB) were outcompeted. With 2.2 mg/L NO_3^--N in the influent water, the fraction of HB increased from less than 3% to 23.85%. However, the fraction of AMO and CRB decreased from 46% and 33% to less than 15% and 5%, respectively. The decrease of chromate reducers in our system is mainly due to their slow kinetics of nitrate utilization. Subsequent model analysis showed that chromate removal efficiency can be strengthened by biofilm thickness control and DO management. A biofilm thickness of 150 μm and an influent DO concentration of 0.5 mg-O_2/L could enhance the performance of the MBfR under the simulated conditions in this work.

Declaration of competing interest

The authors declare that they have no known competing financial interests or personal relationships that could have appeared to influence the work reported in this paper.

Acknowledgments

The authors greatly thank the “National Natural Science Foundation of China (Grant No. 51878596, 21577123)”, the “Natural Science Funds for Distinguished Young Scholar of Zhejiang Province (LR17B070001)”, and the “National Key Technology R&D Program (2018YFC1802203)” for their financial support.

Appendix A. Supplementary data

Supplementary data to this article can be found online at https://doi.org/10.1016/j.wroa.2019.100037.

References

Alrashed, W., Lee, J., Park, J., Rittmann, B.E., Tang, Y.N., Neufeld, J.D., Lee, H.S., 2018. Hypoxic methane oxidation coupled to denitrification in a membrane biofilm. Chem. Eng. J. 348, 745–753. https://doi.org/10.1016/j.cej.2018.04.202.

Ahmed, T., Semmens, M.J., 1992. The use of independently sealed microporous hollow fiber membranes for oxygenation of water: model development. J. Membr. Sci. 69, 11–20. https://doi.org/10.1016/0376-7388(92)80163-E.

Camargo, F.A., Bento, F.M., Okeke, B.C., Frankenberger, W.T., 2003. Chromate reduction by chromium-resistant bacteria isolated from soils contaminated with dichromate. J. Environ. Qual. 32, 1228. https://doi.org/10.2134/jeq2003.1228.

Chen, J., Strous, M., 2013. Denitrification and aerobic respiration, hybrid electron transport chains and co-evolution. Biochim. Biophys. Acta 1827, 136–144. https://doi.org/10.1016/j.bbabio.2012.10.002.

Chen, X.M., Ni, B.J., 2016. Model-based evaluation on simultaneous nitrate and arsenite removal in a membrane biofilm reactor. Chem. Eng. Sci. 152, 488–496. https://doi.org/10.1016/j.ces.2016.06.049.

Chen, X.M., Guo, J.H., Xie, G.J., Yuan, Z.G., Ni, B.J., 2016. Achieving complete nitrogen removal by coupling nitritation-anammox and methane-dependent denitrification: a model-based study. Biotechnol. Bioeng. 113, 1035–1045. https://doi.org/10.1002/bit.25866.

EPA, 2009. National primary drinking water standards. EPA 816-F-09-004, Washington, DC. https://doi.org/10.1017/cbo9780511805387.034.

Floch, Martin H., 2013. Present knowledge in nutrition, 10th edition. J. Clin. Gastroenterol. 47, 373. https://doi.org/10.1097/mcg.0b013e31827943b3.

Henze, M., Gujer, W., Mino, T., Van Loosedrecht, M., 2000. Activated Sludge Models ASM1, ASM2, ASM2d and ASM3. TJ International, Cornwall, UK.

Horn, H., Lackner, S., 2014. Modeling of biofilm systems: a review. Adv. Biochem. Eng. Biotechnol. 146, 53–76. https://doi.org/10.1007/10_2014_275.

Lackner, S., Terada, A., Smets, B.F., 2008. Heterotrophic activity compromises autotrophic nitrogen removal in membrane-aerated biofilms: results of a modeling study. Water Res. 42, 1102–1112. https://doi.org/10.1016/j.watres.2007.08.025.

Lai, C.Y., Zhong, L., Zhang, Y., Chen, J.X., Wen, L.L., Shi, L.D., Sun, Y.P., Ma, F., Rittmann, B.E., Zhou, C., Tang, Y.N., Zheng, P., Zhao, H.P., 2016a. Bioreduction of chromate in a methane-based membrane biofilm reactor. Environ. Sci. Technol. 50, 5832–5839. https://doi.org/10.1021/acs.est.5b06177.

Lai, C.Y., Wen, L.L., Shi, L.D., Zhao, K.K., Wang, Y.Q., Yang, X.E., Rittmann, B.E., Zhou, C., Tang, Y.N., Zheng, P., Zhao, H.P., 2016b. Selenate and nitrate bioreductions using methane as the electron donor in a membrane biofilm reactor. Environ. Sci. Technol. 50, 10179–10186. https://doi.org/10.1021/acs.est.6b02807.

Lai, C.Y., Dong, Q.Y., Chen, J.X., Zhu, Q.S., Yang, X., Chen, W.D., Zhao, H.P., 2018. Role of extracellular polymeric substances in a methane based membrane biofilm reactor reducing vanadate. Environ. Sci. Technol. 52, 10680–10688. https://doi.org/10.1021/acs.est.8b02374.

Laspidou, C.S., Rittmann, B.E., 2002. A unified theory for extracellular polymeric substances, soluble microbial products, and active and inert biomass. Water Res. 36, 2711–2720. https://doi.org/10.1016/s0043-1354(01)00413-4.

Lin, Y.H., Wu, C.L., Hsu, C.H., Li, H.L., 2009. Biodegradation of phenol with chromium(VI) reduction in an anaerobic fixed-biofilm process—kinetic model and reactor performance. J. Hazard Mater. 172, 1394–1401. https://doi.org/10.1016/j.jhazmat.2009.08.005.

Liu, Y., Jin, R.F., Liu, G.F., Tian, T., Zhou, J.T., 2017. Effects of hexavalent chromium on performance, extracellular polymeric substances and microbial community structure of anaerobic activated sludge in a sequencing batch reactor. J. Chem. Technol. Biotechnol. 92, 2719–2739. https://doi.org/10.1002/jctb.5294.

Long, M., Zhou, C., Xia, S.Q., Guadiea, A., 2017. Concomitant Cr(VI) reduction and Cr(III) precipitation with nitrate in a methane/oxygen-based membrane biofilm reactor. Chem. Eng. J. 315, 58–66. https://doi.org/10.1016/j.cej.2017.01.018.

Luo, Y.H., Chen, R., Wen, L.L., Meng, F., Zhang, Y., Lai, C.Y., Rittmann, B.E., Zhao, H.P., Zheng, P., 2015. Complete perchlorate reduction using methane as the sole electron donor and carbon source. Environ. Sci. Technol. 49, 2341–2349. https://doi.org/10.1021/es504990m.

Lv, P.L., Shi, L.D., Wang, Z., Rittmann, B.E., Zhao, H.P., 2019. * Methane oxidation coupled to perchlorate reduction in a membrane biofilm batch reactor. Sci. Total Environ. 667, 9–15. https://doi.org/10.1016/j.scitotenv.2019.02.330.

Martin, K.J., Nerenberg, R., 2012. The membrane biofilm reactor (MBfR) for water and wastewater treatment: principles, applications, and recent developments. Bioresour. Technol. 122, 83–94. https://doi.org/10.1016/j.biortech.2012.02.110.

Modin, O., Fukushi, K., Yamamoto, K., 2008. Simultaneous removal of nitrate and pesticides from groundwater using a methane-fed membrane biofilm reactor. Water Sci. Technol. 58, 1273–1279. https://doi.org/10.2166/wst.2008.481.

Modin, O., 2018. A mathematical model of aerobic methane oxidation coupled to denitrification. Environ. Technol. 39, 1217–1225. https://doi.org/10.1080/09593330.2017.1323961.

Nerenberg, R., Rittmann, B.E., Najm, I., 2002. Perchlorate reduction in a hydrogen-based membrane-biofilm reactor. Am. Water Works Assoc. 94, 103–114. https://doi.org/10.1002/j.1551-8833.2002.tb10234.x.

Nerenberg, R., 2016. The membrane-biofilm reactor (MBfR) as a counter-diffusional biofilm process. Curr. Opin. Biotechnol. 38, 131–136. https://doi.org/10.1016/j.copbio.2016.01.015.

Ni, B.J., Yuan, Z.G., 2013. A model-based assessment of nitric oxide and nitrous oxide production in membrane-aerated autotrophic nitrogen removal biofilm systems. J. Membr. Sci. 428, 163–171. https://doi.org/10.1016/j.memsci.2012.10.049.

Ni, B.J., Smets, B.F., Yuan, Z.G., Pellicer-Nàcher, C., 2013. Model-based evaluation of the role of Anammox on nitric oxide and nitrous oxide productions in membrane aerated biofilm reactor. J. Membr. Sci. 446, 332–340. https://doi.org/10.1016/j.memsci.2013.06.047.

Pattanapipitpaisal, P., Brown, N., Macaskie, L., 2001. Chromate reduction and 16S rRNA identification of bacteria isolated from a Cr(VI)-contaminated site. Appl. Microbiol. Biotechnol. 57, 257–261. https://doi.org/10.1007/s002530100758.

Peng, L., Liu, Y.W., Gao, S.H., Chen, X.M., Ni, B.J., 2016. Evaluating simultaneous chromate and nitrate reduction during microbial denitrification processes. Water Res. 89, 1–8. https://doi.org/10.1016/j.watres.2015.11.031.

Reichert, P., 1994. AQUASIM-a tool for simulation and data analysis of aquatic systems. Water Sci. Technol. 30, 21–30. https://doi.org/10.2166/wst.1994.0025.

Reichert, P., 1998. AQUASIM 2.0- User Manual. EAWAG, Switzerland.

Rittmann, B.E., Mccarty, P.L., 2002. Environmental Biotechnology : Principles and Applications. McGraw-Hill, New York.

Shanker, A.K., Cervantes, C., Lozatavera, H., Avudainayagam, S., 2005. Chromium toxicity in plants. Environ. Int. 31, 739–753. https://doi.org/10.1016/j.envint.2005.02.003.

Skowlund, C.T., 1990. Effect of biofilm growth on steady-state biofilm models. Biotechnol. Bioeng. 35, 502–510. https://doi.org/10.1002/bit.260350508.

Srivastava, S., Prakash, S., Srivastava, M.M., 1999. Chromium mobilization and plant availability - the impact of organic complexing ligands. Plant Soil 212, 201–206. https://doi.org/10.1023/A:1004691217480.

Sun, J., Dai, X., Peng, L., Liu, Y., Wang, Q., Ni, B.J., 2017. A biofilm model for assessing perchlorate reduction in a methane-based membrane biofilm reactor. Chem. Eng. J. 327, 555–563. https://doi.org/10.1016/j.cej.2017.06.136.

Tang, Y.N., Zivel, M., Zhou, C., Shin, J.H., Ahn, C.H., Meyer, K., Candelaria, D., Friese, D., Overstreet, R., Scott, R., 2010. Bioreduction of nitrate in groundwater using a pilot-scale hydrogen-based membrane biofilm reactor. Front. Environ. Sci. Eng. China 4, 280–285. https://doi.org/10.1007/s11783-010-0235-9.

Tang, Y.N., Zhao, H.P., Marcus, A.K., Krajmalnik, B.R., Rittmann, B.E., 2012. A steady-state biofilm model for simultaneous reduction of nitrate and perchlorate, part 1: model development and numerical solution. Environ. Sci. Technol. 46, 1598–1607. https://doi.org/10.1021/es203129s.

Tang, Y.N., Ontiveros, V.A., Feng, L., Zhou, C., Krajmalnik, B.R., Rittmann, B.E., 2013. A biofilm model to understand the onset of sulfate reduction in denitrifying membrane biofilm reactors. Biotechnol. Bioeng. 110, 763–772. https://doi.org/10.1002/bit.24755.

Tekerlekopoulou, A.G., Tsiflikiotou, M., Akritidou, L., Viennas, A., Tsiamis, G., Pavlou, S., Bourtzis, K., Vayenas, D.V., 2013. Modelling of biological Cr(VI) removal in draw-fill reactors using microorganisms in suspended and attached growth systems. Water Res. 47, 623–636. https://doi.org/10.1016/j.watres.2012.10.034.

Wanner, O., Gujer, W., 1986. A multispecies biofilm model. Biotechnol. Bioeng. 28, 314–328. https://doi.org/10.1002/bit.260280304.

Wanner, O., Reichert, P., 1996. Mathematical modeling of mixed-culture biofilms. Biotechnol. Bioeng. 49, 172–184. https://doi.org/10.1002/(sici)1097-0290(19960120)49:2<172::aid-bit6>3.3.co;2-6.

Zhai, S.Y., Zhao, Y.X., Ji, M., Qi, W.F., 2017. Simultaneous removal of nitrate and chromate in groundwater by a spiral fiber based biofilm reactor. Bioresour. Technol. 232, 278–284. https://doi.org/10.1016/j.biortech.2017.01.076.

Zhong, L., Lai, C.Y., Shi, L.D., Wang, K.D., Dai, Y.J., Liu, Y.W., Ma, F., Rittmann, B.E., Zheng, P., Zhao, H.P., 2017. Nitrate effects on chromate reduction in a methane-based biofilm. Water Res. 115, 130–137. https://doi.org/10.1016/j.watres.2017.03.003.